

Spectroscopic properties of Yb^{3+} : LuLiF_4 crystal grown by the Czochralski method for laser applications and evaluation of quenching processes: a comparison with Yb^{3+} : YLiF_4

A. Bensalah^{a,b,*}, Y. Guyot^a, A. Brenier^a, H. Sato^b, T. Fukuda^b, G. Boulon^{a,b}

^a *Physics and Chemistry of Luminescent Materials, UMR 5620 CNRS, Claude Bernard/Lyon 1 University, 69622 Villeurbanne, France*

^b *Institute of Multidisciplinary Research for Advanced Materials, Tohoku University, 2-1-1 Aobaku, Katahira Sendai 980-8577, Japan*

Abstract

Spectroscopic properties of Yb^{3+} ion in LuLiF_4 (LLF) laser host are presented here for the first time. Czochralski technique was used to grow undoped and Yb^{3+} -doped LLF single crystals under CF_4 atmosphere. Detailed analysis of Yb^{3+} -doped LLF spectroscopy were made to contribute to the determination of energy levels in this host and a comparison with the isomorphic YLiF_4 (YLF) laser host is done. We are dealing with temperature and concentration dependences of both π and σ polarizations of the infrared (IR) absorption and emission spectra. Raman spectra were also used to give an attempt for the interpretation of electronic and vibronic levels. Concentration dependence of fluorescence lifetimes allows the measurement of the high radiative lifetime in the range of 2–3 ms and shows a strong self-trapping process. Self-quenching was not seen by the reduction of the decay times but observed by non-radiative up-conversion energy transfer due to the presence of Er^{3+} and Tm^{3+} ions as unexpected impurities. Contrary to oxide crystals this process still remains lower than the self-trapping process. Yb^{3+} pairing and clustering were investigated as well. Evaluation of the laser potentiality of this host by the evaluation of figure-of-merit developed by our group is presented.

© 2004 Elsevier B.V. All rights reserved.

Keywords: Laser crystals; Yb^{3+} -doped LuLiF_4 ; Energy levels; Quenching process

1. Introduction

Yb^{3+} is indeed the most promising ion that can be used in a non- Nd^{3+} laser in the near-IR spectral around 1030 nm for all solid-state laser sources under InGaAs laser diode pumping between 900 and 980 nm. The Yb^{3+} ion has several advantages compared with Nd^{3+} ion due to its very simple energy level scheme, constituting of only two $^2\text{F}_{7/2}$ and $^2\text{F}_{5/2}$ levels. There is no excited state absorption, no cross-relaxation process and no more up-conversion internal mechanism able to reduce the effective laser cross-section and, in addition, the intense and broad Yb^{3+} absorption lines are well suited for IR laser diode pumping.

Our group has been investigating, during these latest years, the spectroscopic properties of several Yb^{3+} -doped single crystal oxides and a new general method of evaluation was pointed out depending on the oscillator or the

amplifier regimes [1,2]. In order to be completed, this study should include fluoride single crystals, another crystal family very useful for optical applications like laser sources. Indeed, fluorides single crystals are interesting because of their high transparency in a wide wavelength region from the VUV to the IR, low refractive index limiting non-linear effects under intense laser sources pumping and low phonon energy, which increases the radiative emission probability of the active ions. We already submitted in a recent paper, an investigation of the spectroscopic properties of Yb^{3+} in YLF [3]. In the present work, spectroscopic properties of Yb^{3+} ion are reported, for the first time to our knowledge, in the fluoride host LLF grown by the Czochralski method and compared with those of YLF.

Only few works have been published on LLF single crystal probably because the cost of LuF_3 raw material is too high. LLF host material doped with different rare earth Pr^{3+} , Ce^{3+} or Nd^{3+} was investigated mainly as scintillators or tunable UV solid-state laser [4–9]. More recently, LLF doped with Tb^{3+} was also considered as new VUV light source for lithographic applications [10].

* Corresponding author. Tel.: +33-4-7243-2970.

E-mail address: bensalah@pcml.univ-lyon1.fr (A. Bensalah).

To the contrary, YLF has been widely studied as a laser material and generally for such application, similar lasing properties in YLF and LLF are expected since they are isomorphous. However, recent works involving materials with Lu^{3+} instead of Y^{3+} or codoped with Yb^{3+} ions showed reduced solarization effects and improved laser performance [11–14]. Indeed, it has been shown that Ce:LLF exhibits much better laser performance than Ce:YLF [15]. In the case of Nd doping as well, LLF system has a 1047 nm emission bandwidth 25% larger than Nd:YLF, which makes it very promising for laser mode-locked operation [16]. Moreover, in a recent work [17], Tm-Ho co-doped LLF showed better laser performance than YLF as eye safe laser at 2 μm . Therefore, we investigated Yb^{3+} -doped LLF as a laser material and compared it with Yb^{3+} -doped YLF.

The interpretation of the Yb^{3+} energy levels in YLF turned out to be difficult because of the re-absorption feature in this fluoride host as well as the strong phonon–electron coupling of Yb^{3+} ion. Using absorption, emission and Raman spectroscopy measurements at RT and 12 K, an attempt of Yb^{3+} energy levels assignment was proposed. Same approach is followed in the present work for Yb^{3+} -doped LLF and a systematic comparison with Yb^{3+} -doped YLF is done. In addition, evaluation of the quenching process by investigating radiative and non-radiative energy transfers in this fluoride host is made.

2. Experimental techniques

Crystal growth was performed in a vacuum-tight Czochralski system with high-purity graphite resistive heater and thermal insulators. The starting materials were prepared from high-purity commercial fluoride powders of LiF and LuF_3 (>99.99%). As dopants, YbF_3 powders of high purity (>99.99%). LLF compound melts congruently, but in order to compensate LiF evaporation the initial

composition was 2 mol% of LiF enriched from the stoichiometric one. The basic compounds and the dopants were melted in a platinum crucible with 60 mm in diameter. The pulling rate was 1 mm/h and the rotation rate was 15 rpm. Growth orientations were controlled using the a -axis oriented undoped YLF seed crystal. Prior to filling with gas and melting the charge, the growth chamber was evacuated to 10^{-4} Pa and heated to 700 °C for a period of 12 h. Such treatment was carried out to eliminate water and/or oxygen from the chamber and the starting materials [18]. High-purity CF_4 gas (99.9999%) was slowly introduced into the furnace. The mixtures were melted under this atmosphere. After growth, the crystals were cooled down to room temperature at a rate of 30 °C/h.

Samples for spectroscopic measurements were cut parallel to the optical c -axes and polished. Absorption spectra were recorded with a spectrophotometer (Perkin Elmer lambda 9000) equipped with a cryostat allowing measurements between 12 K and room temperature. Excitation of the Yb^{3+} fluorescence was performed with a frequency doubled Nd:YAG laser (10 ns, 10 Hz) pumping a Quantel two-amplifier-stage, dye laser containing a mixture of DCM and LD698 and followed by a hydrogen Raman cell shifter to generate a beam in the 920–960 nm range. The specific infrared fluorescence is selected by using a Jobin Yvon HRS1 monochromator fit with a 600 grooves/mm grating blazed at 1 μm . The signal is detected by a slow North Coast germanium cell, cooled by liquid nitrogen, and sent into a Stanford boxcar averager SRS 250. The decay kinetics were recorded with a Lecroy LT 342 digital oscilloscope connected to a fast North Coast germanium cell. The Raman spectra were recorded by a DILOR XY triple monochromator with a multi-channel charge-coupled (CCD) detector.

Detection of the photoluminescence in the visible was performed using an intensified CCD camera coupled with an Oriel monochromator with a 1200 grooves/mm grating associated to a Stanford delay generator.

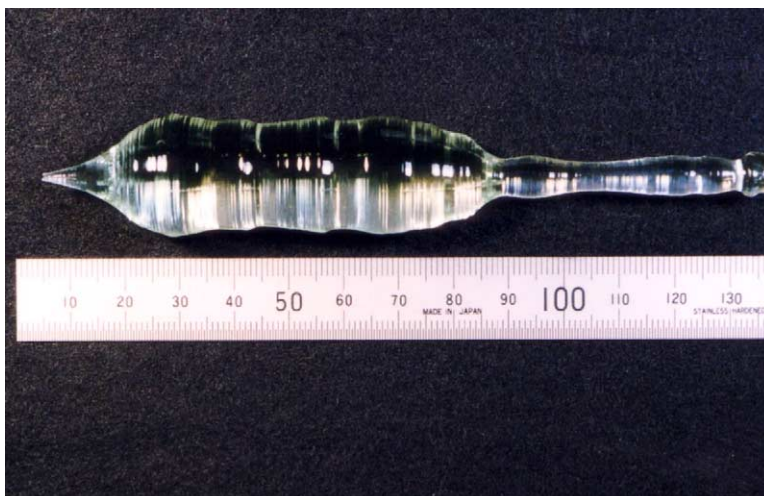


Fig. 1. 5% Yb^{3+} -doped LuLiF_4 single crystal with 1 in. in diameter grown by the Czochralski method.

3. Results and discussions

3.1. Crystal growth

When powder raw materials were melted, a black scum was observed floating on the melt surface. This film is due to the oxygen and carbon contamination of the raw materials [19]. However, a clean and transparent melt was obtained after removing the scum by scraping the solidified surface and subsequently re-melting the compound. The growth of LLF crystals was easier than YLF. Indeed, LLF is congruent with $T_f = 825^\circ\text{C}$ while YLF is incongruent (52/48) with $T_f = 842^\circ\text{C}$ leading to less defects, thus to better optical quality [20].

Undoped, 0.5 and 5% Yb^{3+} -doped LLF single crystals were successfully grown and Fig. 1 shows the as-grown

5% Yb^{3+} -doped LLF crystal with dimensions of 18 mm in diameter and 70 mm in length. Obtained crystals were transparent free from cracks, bubbles and inclusions.

LLF and YLF have both a scheelite structure with tetragonal system. They crystallise in $I_{41/a}$ (C_{4h}^6) space group but with slightly different lattice parameters ($a = 5.150 \text{ \AA}$, $c = 10.47 \text{ \AA}$ for LLF and $a = 5.155 \text{ \AA}$ and $c = 10.68 \text{ \AA}$ for YLF).

3.2. Characterization and assignment of spectroscopic properties

As in the case of YLF host, two orientations are needed: the π spectra with $E//c$ and the σ spectra with $E \perp c$ to characterize the electric-dipole transitions since LLF laser host is an uniaxial crystal as well. The emission spectra were

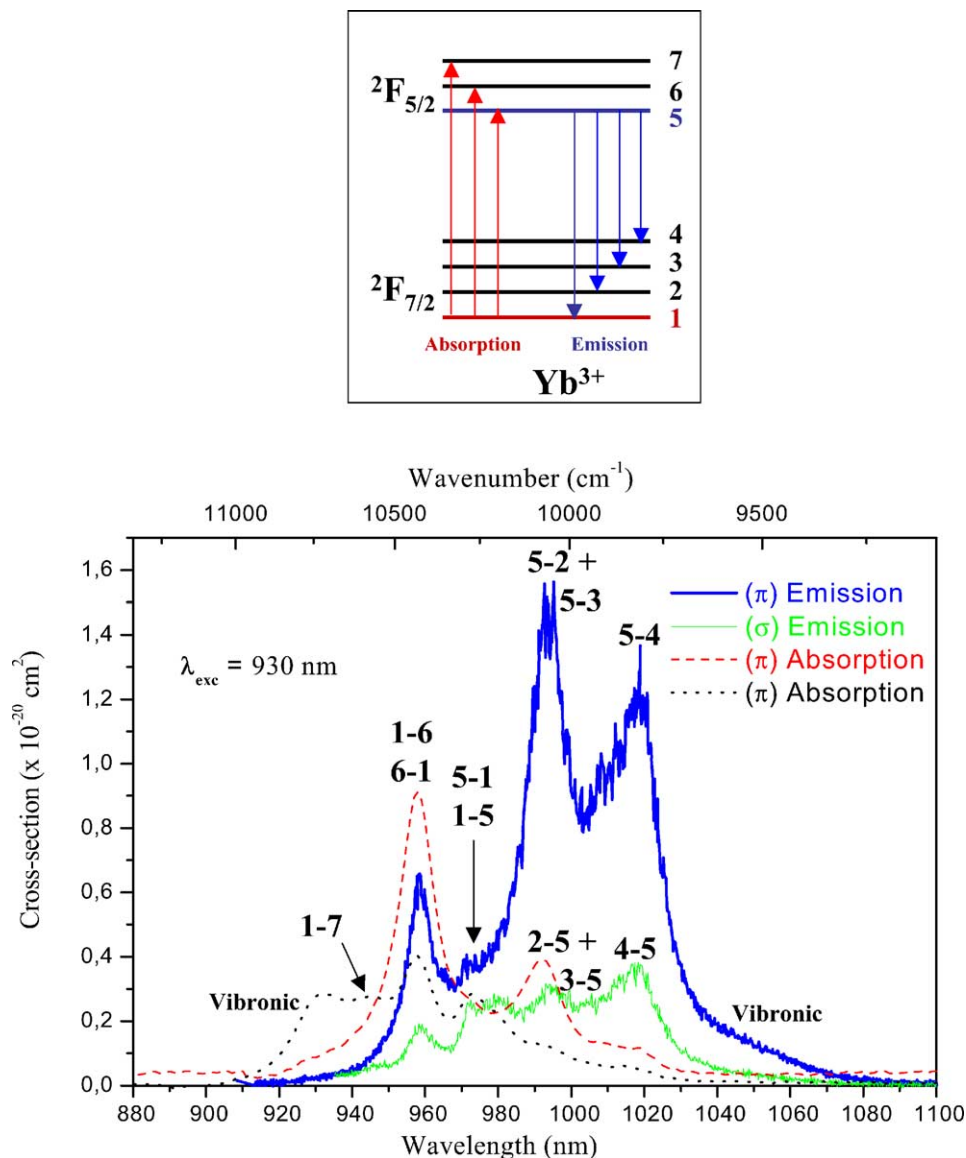


Fig. 2. Polarized absorption and emission cross-section at room-temperature of 0.5% Yb^{3+} -doped LuLiF_4 .

Table 1
Decay time values of Yb^{3+} in LuLiF_4 and YLiF_4 at RT and 12K

Sample	Decay time at RT (ms)	Decay time at 12K (ms)
5%Yb:LLF RT	2.61	1.88
0.5%Yb:LLF RT	2.03	1.80
10%Yb:YLF RT	3.18	2.25
0.5%Yb:YLF RT	2.14	1.94

obtained from the Fuchtbauer–Ladensburg method with decay times measured at 12 K for 0.5% Yb^{3+} as reported in Table 1. The polarized absorption and the emission (π and σ) spectra of the 0.5% Yb^{3+} -doped LLF at room temperature (RT) under pumping at 930 nm, in the vibronic part of the highest Stark level ($1 \rightarrow 7$), are plotted in Fig. 2. Several bands can be seen in both absorption and emission due to the different transitions between Stark levels of the ground $^2F_{7/2}$ state and the excited $^2F_{5/2}$ one. These Stark levels are labelled from 1 to 4 in the ground state and from 5 to 7 in the excited state from the lowest to the highest energy as can be seen in the inset of Fig. 2. Same observations and comments can be done as for Yb^{3+} -doped YLF [17]. LLF host reveals a comparable weak crystal field with YLF. In the case of LLF host, the values of absorption and emission cross-sections ($0.9 \times 10^{-20} \text{ cm}^2$ at 958 nm ($E//c$) and $1.5 \times 10^{-20} \text{ cm}^2$ at 995 nm ($E//c$)) are slightly larger than for YLF ($0.9 \times 10^{-20} \text{ cm}^2$ at 960 nm ($E//c$) and $1.3 \cdot 10^{-20} \text{ cm}^2$ at 995 nm ($E//c$)), respectively. The position of the bands observed in absorption and emis-

Table 2
 Yb^{3+} energy levels in LLF and YLF at 12 K

Yb^{3+} energy levels	LuLiF_4 (cm^{-1})	YLiF_4 (cm^{-1})
1	0	0
2	215	218
3	243	248
4	486	485
5	10290	10293
6	10438	10416
7	10570	10554

sion, especially at 12 K (Fig. 5), are slightly shifted toward shorter wavelength in LLF than in YLF probably due to the difference in lattice parameters between these two materials.

As for YLF, same difficulties were met for the assignment of Yb^{3+} energy levels in LLF host mainly because the strong electron–photon coupling of Yb^{3+} ion, which results in the appearance of additional peaks making the interpretation of the different absorption and emission lines complex especially at RT. Moreover, re-absorption feature is also observed in Yb^{3+} -doped LLF as can be seen in Fig. 3 where the polarized emissions at RT of the 0.5% and the 5% Yb -doped LLF are presented together. The resonant transitions are re-absorbed with the increase of Yb^{3+} concentration in LLF by radiative energy transfer between Yb^{3+} ions, which results in a decrease of the emission cross-sections especially for the band at 958 nm since it has the strongest absorption cross-section at RT. Consequently, a special care

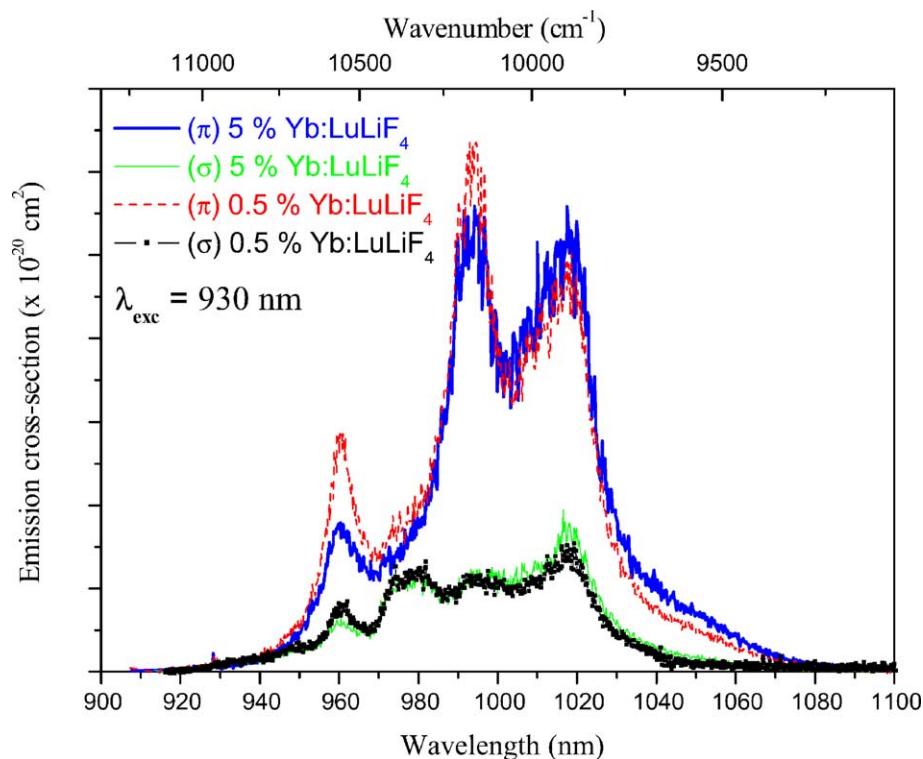


Fig. 3. Polarized emission cross-section of 5 and 0.5% Yb^{3+} -doped LuLiF_4 .

is needed to assign Yb^{3+} absorption and emission transitions in LLF as it was the case in YLF. Since same behaviour was observed in both YLF and LLF, similar analysis were carried out for the interpretation of the results obtained in LLF. Especially the 0-phonon line, which is defined to be the energy separation between the lowest Stark levels of each manifold ($5 \rightarrow 1$ emission transition), was ascribed at 972 nm.

In order to distinguish between electronic and vibronic transitions we compared absorption and emission spectra at low temperature with Raman spectra as described in [17]. In Fig. 4 the three spectra are superposed by taking the origin of the absorption and the emission at the $1 \leftrightarrow 5$ transition, in coincidence with the Rayleigh line of the Ar-laser (514.5 nm) used to record the Raman spectra. We obtained quite different Raman spectra for LLF with respect to YLF. This might be related to the different Lu and Y ions composing LLF and YLF, respectively.

Following the same analysis as for YLF, interpretation of the spectroscopic results of Yb^{3+} -doped LLF was made and an attempt of the Yb^{3+} energy level scheme in this laser host is summarized in the inset of Fig. 5 and Table 2.

Consequently to our interpretation of Yb^{3+} energy levels in LLF, we have then applied the barycentre plot method,

introduced by Antic-Fidancev and described in [21] and placed this laser host on the barycentre plot. Similarly to YLF, LLF also fits well to the theoretical line.

3.3. Excited state dynamics

3.3.1. Radiative and non-radiative energy transfers

The determination of the intrinsic radiative lifetime of Yb^{3+} in crystals requires a lot of precaution. Especially in LLF and YLF where, depending on the concentration, the self-trapping process is much involved, the lifetime measurements were carried out on samples cut and polished in a parallelepiped shape of (1.5 mm \times 1.5 mm \times 10 mm) size. A special attention was paid to measure the fluorescence decays in the same geometrical conditions for each concentration and temperature.

The fluorescence decay time showed an exponential behaviour with a high experimental life time value from 1.94 to 3.18 ms. All the measured values are summarised for both LLF and YLF in Table 1.

As can be seen in Fig. 6, the increase of the decay times up to 10% of Yb^{3+} in YLF, reveals a strong self trapping by radiative energy transfer which is stronger than the

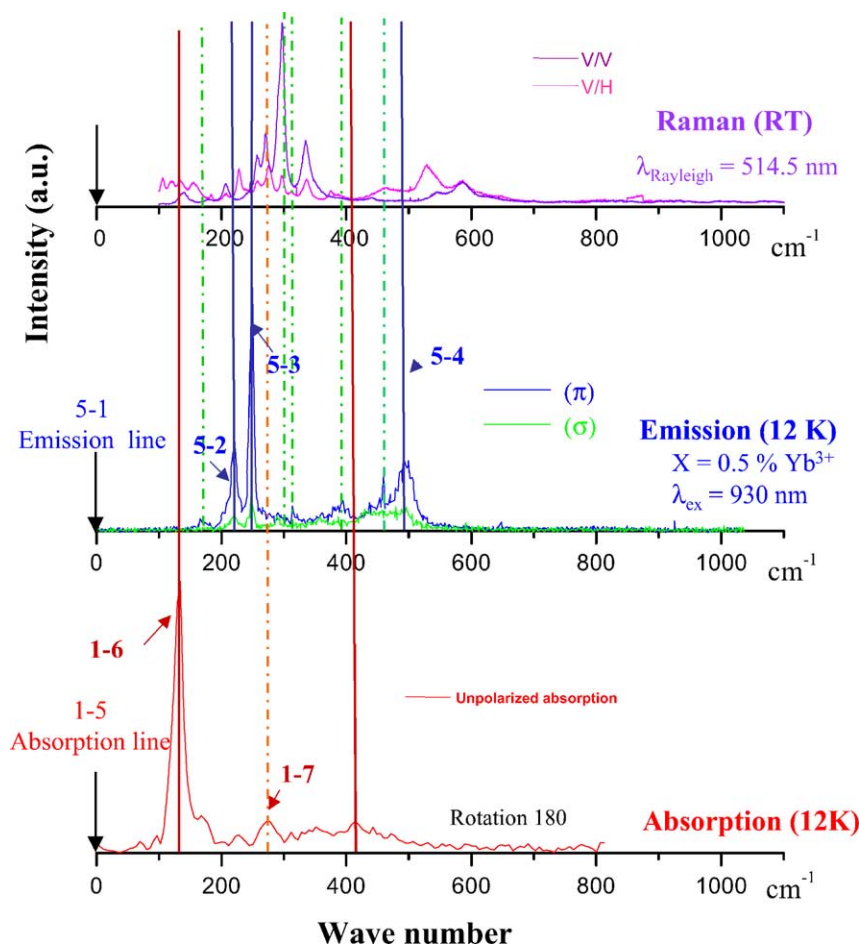


Fig. 4. Interpretation of Yb^{3+} transitions in 0.5% Yb^{3+} -doped LuLiF_4 with the help of absorption, emission and Raman spectra.

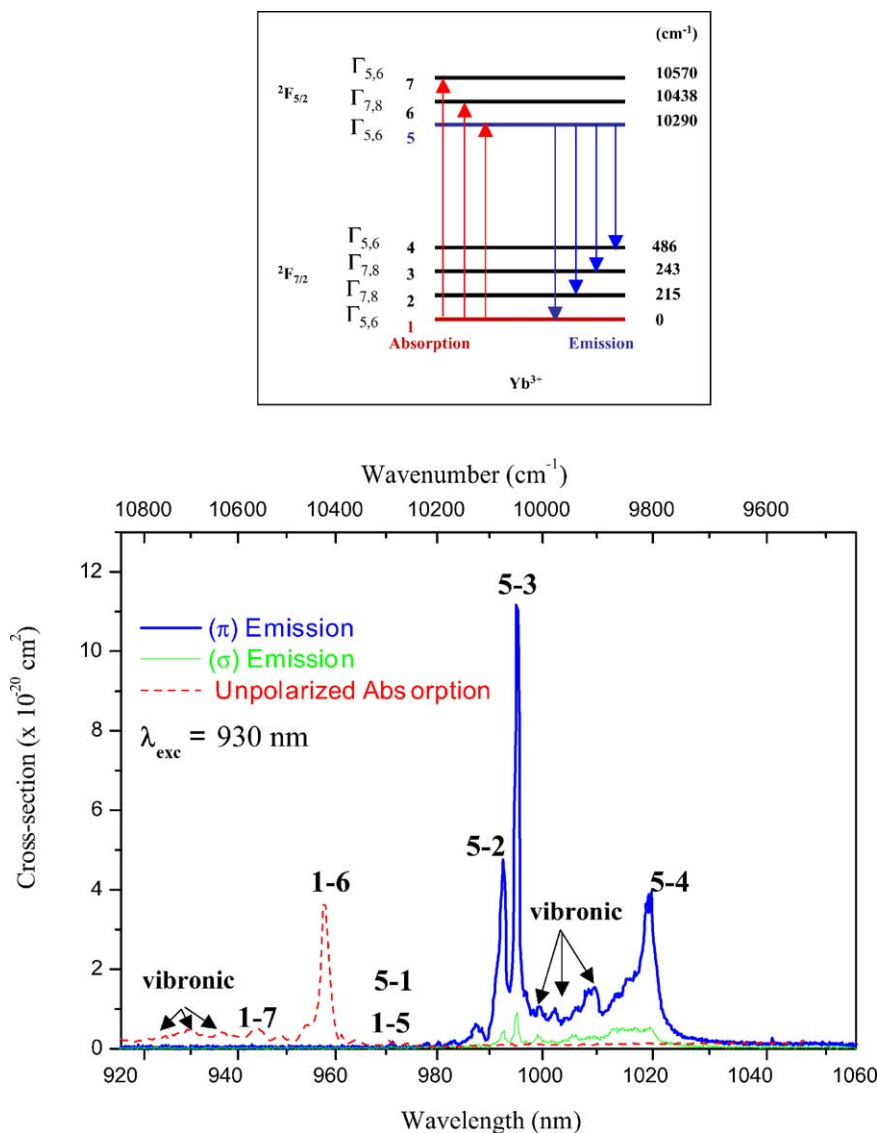
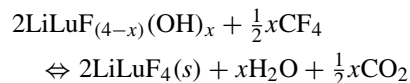


Fig. 5. Polarized absorption and emission cross-sections at 12K of 0.5%Yb³⁺-doped LuLiF₄.

non-radiative energy transfer or self-quenching, at least up to 10%. Besides, the experimental decay time value is increasing with the increase of the temperature contrary to the oxide hosts which reveals again a strong self-trapping. Similar increase of the decay time with the concentration was observed up to 17%Yb³⁺ in CaF₂ grown either by LHPG method or by simple melting method [22], which is a higher value with respect to sesquioxides and YAG about 5%Yb³⁺ for instance [23–27]. Fig. 6 shows only the comparison with CaF₂ fluoride host.

Interpretation of the radiative energy transfer was already published [1,23,28,29]. This higher Yb³⁺ concentration limit for the increase of the decay time in fluorides is apparently due to a weaker non-radiative energy transfer effect or self-quenching than in oxides because of their lower phonon energy. One additional possible explanation might be related to the fact that we do not observe OH⁻ complexes in fluorides with respect to oxides. Indeed, during the growth

of fluorides single crystals under CF₄ atmosphere, OH⁻ complexes are eliminated following the equations below



In fact, the presence of OH⁻ complexes, observed mainly in oxides, contribute to the de-excitation of Yb³⁺ by non-radiative mechanism which results in the decrease of the total decay time.

Since the decay times were increasing with the Yb³⁺ concentration up to 10% in YLF (Fig. 6), we could not detect the self-quenching which in effect consists of a decrease of the life time as it was observed in many other laser hosts

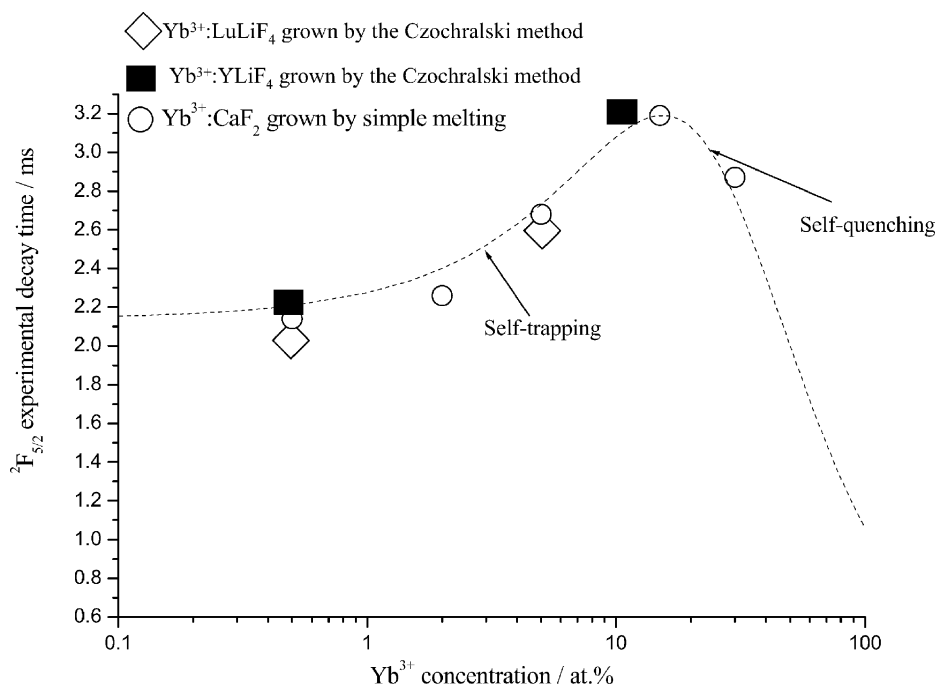


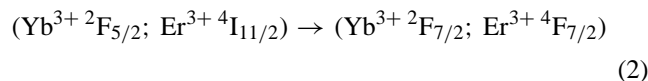
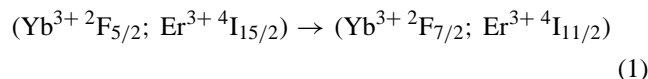
Fig. 6. Concentration dependence of the $\text{Yb}^{3+} \ ^2\text{F}_{5/2}$ excited level in LLF and YLF fluoride hosts as compared with CaF_2 host synthesized by simple melting [22].

[23–26,30] due to the traces of unexpected impurities as rare earth ions (RE) and OH^- complexes. However, non-radiative energy transfer was clearly observed by up-conversion process from excited Yb^{3+} ions to the Tm^{3+} and Er^{3+} unexpected impurity ions present in the fluoride crystals, under IR pumping at 930 nm (Fig. 7). Although all starting material used for the crystal growth have a purity of 99.99%, we could not avoid the presence of these RE impurities which even in the order of ppm show a clear fluorescence as shown in Fig. 7 for the 5% Yb-doped LLF.

Looking at the Dieke diagram (Fig. 8), one can see that many resonant and non-resonant energy transfer are possible between trivalent RE ions. Indeed, energy transfers between Yb^{3+} and Er^{3+} or Tm^{3+} are well known [29,31]. Especially in the $10,000 \text{ cm}^{-1}$ energy range, matching with excited state of Yb^{3+} , energy transfers are allowed with the different excited levels of Er^{3+} and Tm^{3+} ions giving rise to several peaks in the visible as it is clearly seen in Fig. 7.

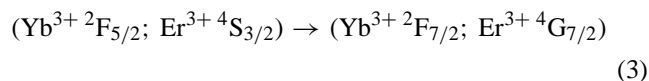
In the case of Yb^{3+} - Er^{3+} , several emissions by resonant energy transfer occurs as schematised in Fig. 8:

The green and red emission at 540 and 650 nm corresponding to the $^4\text{S}_{3/2} \rightarrow ^4\text{I}_{15/2}$ and $^4\text{F}_{9/2} \rightarrow ^4\text{I}_{15/2}$ are the result of the cross relaxation channel:



followed by the relaxation to $^4\text{S}_{3/2}$ and $^4\text{F}_{9/2}$ levels, respectively.

The emissions in the blue-violet range at 365, 380 and 410 nm from $^4\text{G}_{9/2}$, $^4\text{G}_{11/2}$ and $^4\text{G}(1)_{9/2}$ toward the $^4\text{I}_{15/2}$ ground level can be explained by a three photon energy transfer process. The third step of this mechanism is as indicated below:



On the other hand, the $^4\text{F}_{9/2}$ level could be populated through $(\text{Yb}^{3+} \ ^2\text{F}_{5/2}; \text{Er}^{3+} \ ^4\text{I}_{13/2}) \rightarrow (\text{Yb}^{3+} \ ^2\text{F}_{7/2}; \text{Er}^{3+} \ ^4\text{F}_{9/2})$ cross relaxation channel after relaxation from $^4\text{I}_{11/2}$ to $^4\text{I}_{13/2}$.

In the case of Yb^{3+} - Tm^{3+} , the up conversion mechanism is a little bit more complicated since there is no Stark levels in resonance with the $^2\text{F}_{7/2} \rightarrow ^2\text{F}_{5/2}$ Yb^{3+} transition. Thus, the Tm^{3+} blue emission at 480nm can be explained by energy transfer from $^2\text{F}_{7/2} \rightarrow ^2\text{F}_{5/2}$ Yb^{3+} absorption transition to a Tm^{3+} vibronic level in resonance with $\text{Yb}^{3+} \ ^2\text{F}_{5/2}$ excited state. This first step is then followed by several non-radiative relaxations and cross-relaxations as can be seen in Fig. 8, in order to reach the $^1\text{G}_4$ level from where the blue emission occurs as a result of $^1\text{G}_4 \rightarrow ^3\text{H}_6$ transition. From the $^1\text{G}_4$ a red emission can also occur corresponding to the $^1\text{G}_4 \rightarrow ^3\text{F}_4$ transition.

Another possibility for the Tm^{3+} blue and red emissions is a direct energy transfer between the $\text{Er}^{3+} \ ^4\text{F}_{7/2}$ and the $\text{Tm}^{3+} \ ^1\text{G}_4$ resonant energy levels.

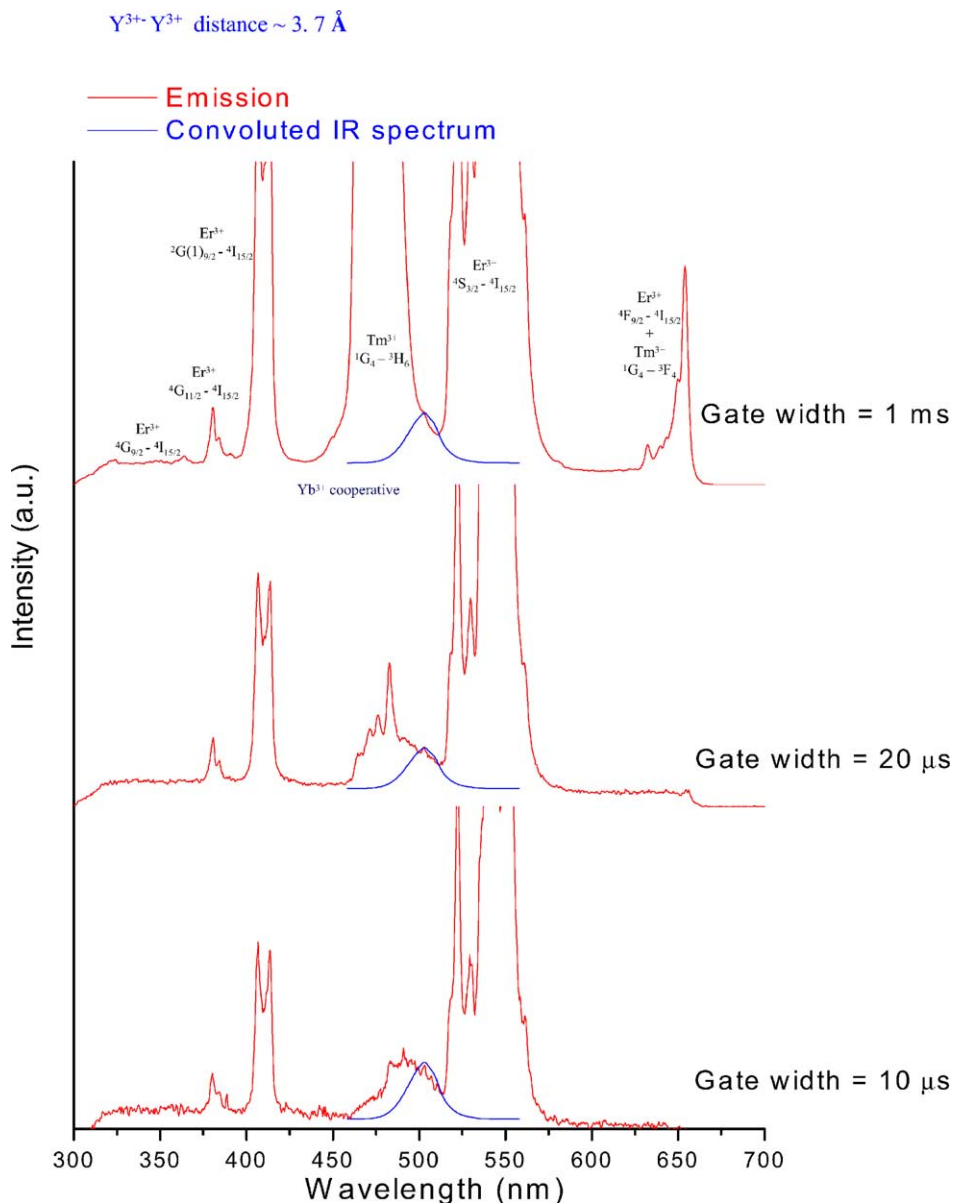


Fig. 7. Up-conversion emission under 930 nm pumping in the 5%Yb³⁺-doped LuLiF₄ at RT using time resolved spectroscopy with a delay of 0 ms for all measurements.

The profiles of the fluorescence decay curves recorded for the RE anti-stokes emission under Yb³⁺ IR pumping presented in Fig. 9, reveal energy transfer both to Er³⁺ at around 540 nm (⁴S_{3/2}-⁴I_{15/2}) and to Tm³⁺ at around 480 nm (¹G₄-³H₆) signed by an initial rise time which disappears under direct excitation in the visible (inset of Fig. 9). This feature is another evidence of the up-conversion process between Yb³⁺ and RE unwanted impurity ions.

3.3.2. Yb³⁺ pair formation

Another mechanism which can play a role in the self quenching mechanism as it has been suggested by Auzel et al. [28] and researched in Y₂O₃ sesquioxide [25] was also searched in our materials. This mechanism is correlated to the possible degree of Yb³⁺ pairing or clustering in Lu³⁺

and Y³⁺ crystallographic sites in LLF and YLF hosts, respectively.

Since Yb³⁺ ion has only one excited state (²F_{5/2}) at about 10 000 cm⁻¹ above the ground state (²F_{7/2}), this ion facilitates the observation of this effect which is characterized by relatively weak visible emission in the green range, that is to say, in the spectral area without any Yb³⁺ absorption. This phenomenon was already observed in YbPO₄ [32], in phosphate glasses [33] and recently in Yb³⁺-doped Y₂O₃ [25] but could not be detected in YLF [34]. Indeed, the authors has explained this first unsuccessful attempt by the ionic character of YLF.

The theoretical predictions of such pairing or clustering were calculated by computing the convolution according to [35]:

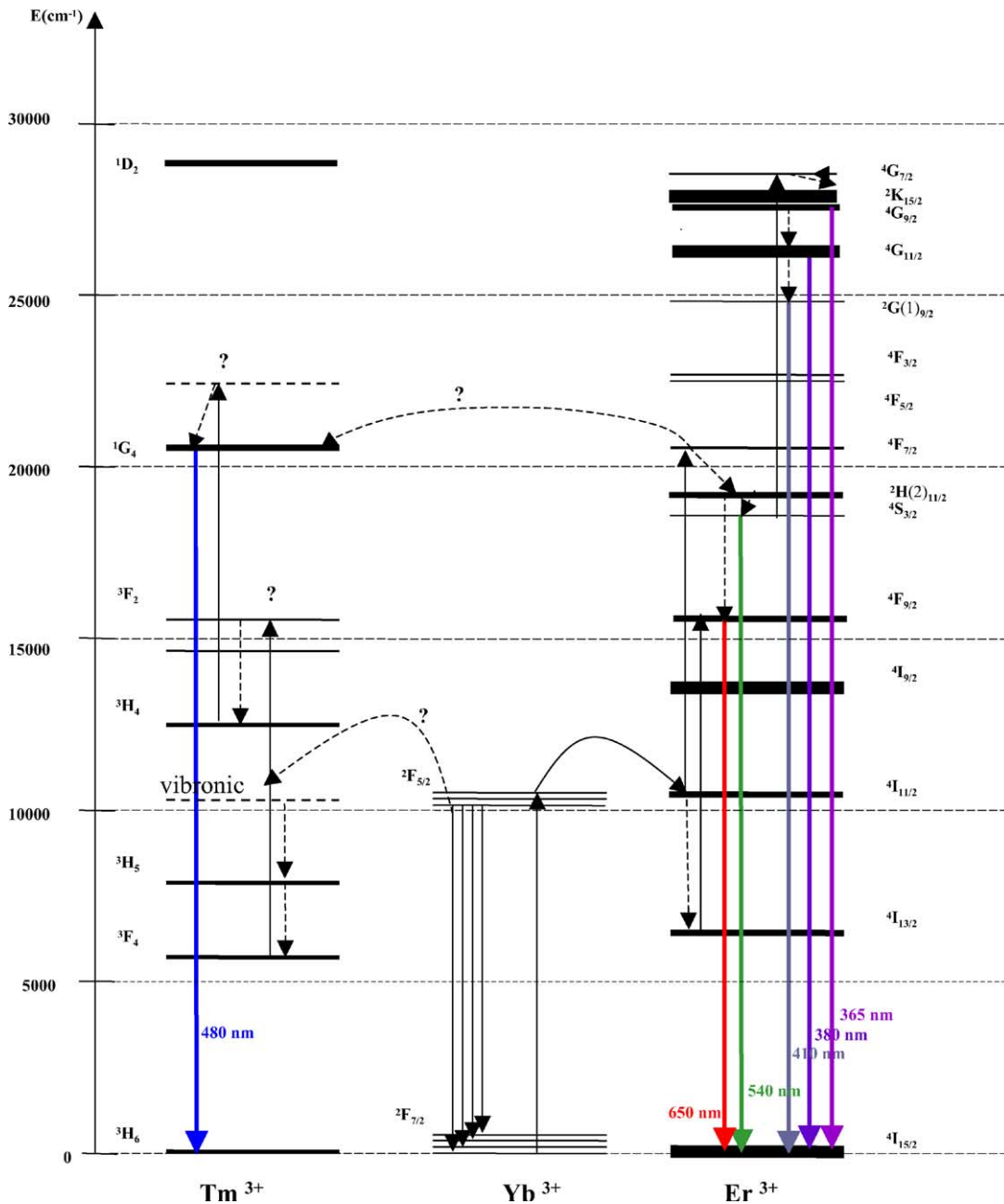


Fig. 8. Dieke diagram: non-radiative energy transfer by up conversion between excited state of Yb³⁺ and Tm³⁺ and Er³⁺ unwanted impurity ions.

$$F(E) = \int_0^\infty f(E')f(E - E') dE'$$

$f(E)$ is the infrared spectrum while $F(E)$ is the expected visible spectrum.

The theoretical curve is shown in Fig. 7. In LLF, where the distance between two Lu ions is in the order of 3.7 Å as for YLF, it was rather difficult to observe the cooperative emission comparing with other materials as Y₂O₃ [25], YAG [27], GGG [36] and CaF₂ [22] studied in the group in which the pair distances are comparable. The observation of the energy transfer by up-conversion effect compared to the

pair luminescence or the cooperative luminescence is indeed, much more probable of several orders of magnitude and so the cooperative emission is covered by the up conversion one. However, by using time resolved spectroscopy in the visible and choosing very small gate width we could detect, in addition to the up-conversion emission from Yb³⁺-Er³⁺ and Yb³⁺-Tm³⁺ energy transfer, the cooperative emission of Yb³⁺ pairs around 500 nm which fits to the theoretical curve (Fig. 7). As mentioned above, visible decay curves of the up-conversion emissions present a rise time. Thus, by looking at shorter times than this rise time, we could isolate the pair emissions. The recorded decay curve at 505 nm

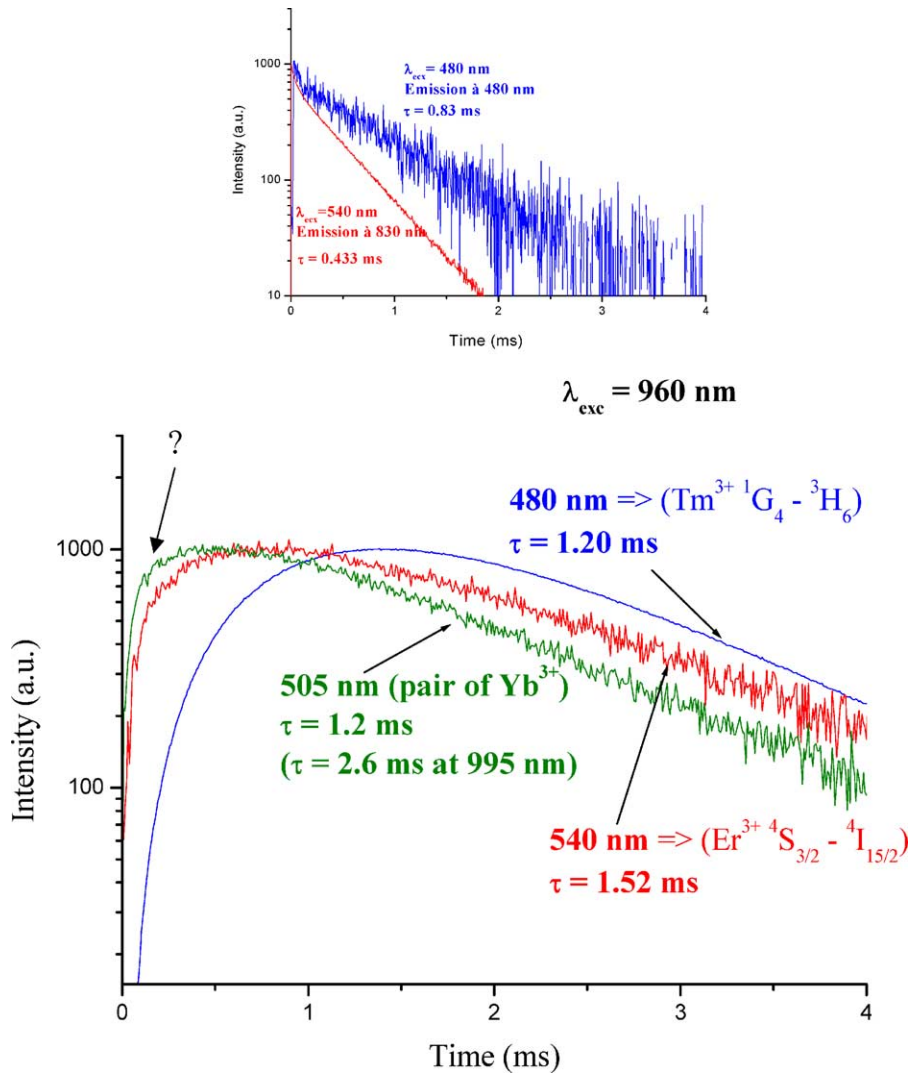


Fig. 9. Decay times of the RE impurity ions in the 5% Yb^{3+} -doped LuLiF_4 under IR excitation.

shown in Fig. 8 for 5% Yb^{3+} -doped LLF corresponds to the expected Yb^{3+} pair or cluster which should be equal to half value of the $^2\text{F}_{5/2}$ level ($\sim 2.6 \text{ ms}$): $[\tau(^2\text{F}_{5/2})/2] \sim 1.3 \text{ ms}$ instead of 1.2 ms measured value].

In principle, the decay curve related to the cooperative emission or pairs should not show any rise time. However, in this case since it was difficult to isolate it from the impurity ions emission, a residual rise time is observed but it is shorter than the one related to the up conversion process as clearly seen in Fig. 9.

The difficulty to point out pairs seems to be related to a higher Yb^{3+} ions homogenous distribution in LLF or YLF grown by the Czochralski method than in CaF_2 or oxides [22].

At last, it is clear that we need to measure Yb^{3+} lifetimes for all concentrations till 100% (LiYbF_4) and to evaluate the quenching mechanisms by comparing with the theoretical model [28]. Further research is in progress.

3.4. First estimations of the laser potentialities

In Fig. 6 are presented the gain cross sections $\sigma_g(\lambda)$ versus wavelength λ at different population inversion β for the 0.5% Yb^{3+} -doped LLF calculated using the following equation:

$$\sigma_g(\lambda) = \beta\sigma_{em}(\lambda) - (1 - \beta)\sigma_{abs}(\lambda)$$

$\sigma_{em}(\lambda)$ and $\sigma_{abs}(\lambda)$ are the emission and absorption cross-sections, respectively.

The gain cross section is usually used to have an idea about the laser potentiality for a given crystal host. For LLF laser host, we obtained similar results as those of YLF with slightly higher gain cross sections since in Yb^{3+} -doped LLF the emission cross section is higher than in Yb^{3+} -doped YLF while the absorption cross section is the same in both crystals. Consequently, one can expect higher laser output in LLF than in YLF.

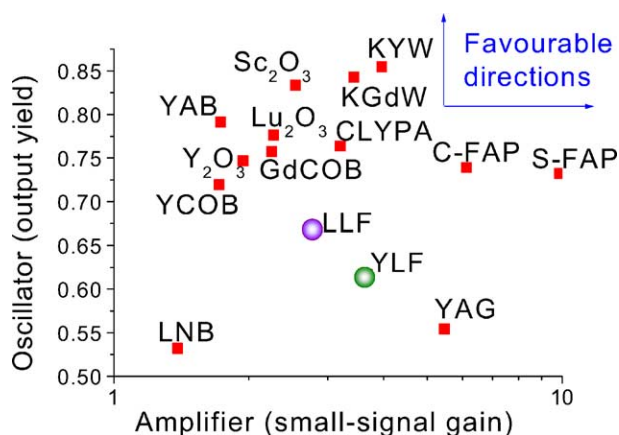


Fig. 10. Evaluation of laser output yield and amplifier small signal gain predicted by the figure-of-merit for LuLiF_4 and YLiF_4 , respectively.

This prediction seems to be confirmed according to the new evaluation of figure-of-merit, developed in the latest years by our group. In fact, based on a quasi-three level laser model described in [2,37,38], several Yb^{3+} -doped laser crystals have been evaluated. The results of calculations are visualized in Fig. 10 in a two-dimensional diagram considering the laser extracted power and the slope efficiency. According to this model a first estimation of the potentiality of Yb^{3+} -doped LLF as laser material in the IR shows that this fluoride has a higher output yield than Yb^{3+} -doped YLF. However, we should take into account the higher price of LuF_3 with respect to YF_3 . Laser tests should be carried out to confirm this prediction.

4. Conclusion

High optical quality single crystals of Yb^{3+} -doped LLF were grown by the CZ method and spectroscopic properties were compared with Yb^{3+} -doped YLF. Re-absorption feature in this fluoride host as well as the strong phonon–electron coupling of Yb^{3+} ion made the assignment of the Yb^{3+} energy levels difficult. Using absorption, emission and Raman spectroscopy measurements at RT and 12 K, an attempt to assign the energy levels of Yb^{3+} ion was proposed. We tried to evaluate the quenching processes in Yb^{3+} -doped LLF by investigating self trapping, self quenching and pairs effect as well. Especially in this crystal, self-trapping effect is much efficient than self-quenching for high Yb^{3+} concentrations contrary to oxides. Finally, the evaluation of Yb^{3+} -doped LLF by one type of figure-of-merit, developed previously, shows its potentiality as laser material with the complementary advantage to be grown with large size and good optical quality since LLF melt congruently while YLF does not. Laser tests on our samples should be carried out to confirm our first estimation.

References

- [1] G. Boulon, A. Brenier, L. Laversenne, Y. Guyot, C. Goutaudier, M.T. Cohen-Adad, G. Métrat, N. Muhlstein, *J. Alloys Compd.* 341 (2002) 2–7.
- [2] A. Brenier, G. Boulon, *J. Alloys Compd.* 210 (2001) 323–324; A. Brenier, G. Boulon, *Europhys. Lett.* 55 (2001) 647.
- [3] A. Bensalah, Y. Guyot, A. Brenier, H. Sato, T. Fukuda, G. Boulon, *Optical Materials*, July 2003, in press.
- [4] S. Nicolas, M. Laroche, S. Girard, R. Moncorgé, Y. Guyot, M.F. Joubert, E. Descroix, A.G. Petrosian, *J. Phys. Condens. Matter.* 11 (1999) 7937.
- [5] M. Laroche, A. Braud, S. Girard, J.L. Doualan, R. Moncorgé, M. Thuau, L.D. Merckle, *J. Opt. Soc. Am. B16* (1999) 2269.
- [6] M. Laroche, J.L. Doualan, S. Girard, J. Margerie, R. Moncorgé, *J. Opt. Soc. Am. B17* (2000) 1291.
- [7] V.V. Semashko, M.F. Joubert, E. Descroix, S. Nicolas, R.Y. Abdulsabirov, A.K. Naumov, S.L. Korableva, A.C. Cefalas, *Proc. SPIE* 4061 (2000) 306.
- [8] Y. Guyot, S. Guy, M.F. Joubert. In: C. Jardin (Ed.), *Suppl. of 'Le vide: Science technique et applications'*, Société française du vide (SFV), Paris, ILLUM'99, p. 13.
- [9] S. Guy, Y. Guyot, A.M. Tkachuk, I.K. Razumova, M.F. Joubert, *J. Phys. IV France* 10 (2000) Pr8.
- [10] E. Sarantopoulou, Z. Kollia, A.C. Cefalas, *Microelectron. Eng.* 61–62 (2002) 133–138.
- [11] M.A. Dubinskii, V.V. Semashko, A.K. Naumov, R.Yu. Abdulsabirov, S.L. Korableva, *Laser Phys.* 4 (1994) 480.
- [12] P. Rambaldi, R. Moncorgé, J.P. Wolf, C. Pédrini, J.Y. Gesland, *Opt. Commun.* 146 (1998) 163.
- [13] M. Laroche, S. Girard, R. Moncorgé, K. Lebbou, T. Fukuda, M. Bettinelli, *CLEO Europ Technol. Digest* 2001, Munich, Germany, June 2001, p. 55.
- [14] V.V. Semashko, M.A. Dubinskii, R.Yu. Abdulsabirov, S.L. Korableva, A.K. Naumov, A.S. Nizamutdinov, M.S. Zhuchkov, in: *Proceedings of the SPIE XI International Feofilov Symposium*, vol. 4766, 24–28 September 2001, Kazan, Russia.
- [15] M.A. Dubinskii, V.V. Semashko, et al., *Laser Phys.* 4 (1994) 480.
- [16] N.D. Vieira Jr, I.M. Ranieri, L.V.G. Tarelho, N.U. Wetter, S.L. Baldochi, L. Gomes, P.S.F. de Matos, W. de Rossi, G.E.C. Nogueira, et al., *J. Alloys Compd.* 344 (2002) 231–239.
- [17] A. Bensalah, K. Shimamura, V. Sudesh, H. Sato, K. Ito, T. Fukuda, *J. Crystal Growth* (2001).
- [18] J.S. Shah, in: B.R. Pamplin (Ed.), *Crystal Growth and Characterisation*, vol. 6. Pergamon Press, Oxford, 1975, p. 144.
- [19] K. Shimamura, S.L. Baldochi, N. Mujilat, K. Nakano, Z. Liu, N. Sarukura, T. Fukuda, *J. Crystal Growth* 211 (2000) 302.
- [20] M. Laroche, S. Girard, R. Moncorgé, M. Bettinelli, R. Abdulsabirov, V. Semashko, *Opt. Mater.* 22 (2003) 147–154.
- [21] E. Antic-Fidancev, *J. Alloys Compd.* 300–301 (2000) 2.
- [22] M. Ito, C. Goutaudier, K. Lebbou, Y. Guyot, T. Fukuda, G. Boulon, *J. Phys.: Condensed Matter*, 10 September 2003.
- [23] L. Laversenne, C. Goutaudier, Y. Guyot, M.Th. Cohen-Adad, G. Boulon, *J. Alloys Compd.* 341 (2002) 214–219.
- [24] L. Laversenne, Y. Guyot, C. Goutaudier, M.Th. Cohen-Adad, G. Boulon, *Opt. Mater.* 17 (2001) 443.
- [25] G. Boulon, L. Laversenne, C. Goutaudier, Y. Guyot, M.T. Cohen-Adad, *J. Luminesc.* 102–103 (2003) 417–425.
- [26] C. Goutaudier, K. Lebbou, Y. Guyot, M. Ito, H. Canibano, L. Laversenne, G. Boulon, *Annales de Chimie—Science des Matériaux*, vol. 28. November–December 2003, pp. 73–88.
- [27] A. Yoshikawa, G. Boulon, L. Laversenne, H. Canibano, K. Lebbou, A. Collombet, Y. Guyot, T. Fukuda, *J. Appl. Phys.* (November 2003).
- [28] F. Auzel, G. Baldachini, L. Laversenne, G. Boulon, *Opt. Mater.* (February 2003), in press.

- [29] F. Auzel, F. Bonfigli, S. Gagliari, G. Baldacchini, *J. Luminesc.* 94–95 (2001) 293–297.
- [30] H. Cañibano, G. Boulon, L. Palatella, Y. Guyot, A. Brenier, M. Voda, R. Balda, J. Fernandez, *J. Luminesc.* 102–103 (2003) 318–326.
- [31] J.S. Haggerty, NASA Report, CR-120948 (1972), C.N.R. Rao Supercond [30].
- [32] E. Nakazawa, S. Shionoya, *Phys. Rev. Lett.* 25 (1970) 1710.
- [33] P. Goldner, B. Schaudel, M. Prassas, F. Auzel, *J. Luminesc.* 87–89 (2000) 688.
- [34] R.T. Wegh, A. Meijerink, *Chem. Phys. Lett.* 246 (1995) 495–498.
- [35] Y. Guyot, R. Moncorge, L.D. Merkle, A. Pinto, B. McIntosh, H. Verdun, *Opt. Mater.* 5 (1996) 127.
- [36] S. Chénais, F. Druon, F. Balembois, P. Georges, A. Brenier, G. Boulon, *Opt. Mater.* 22 (2003) 99.
- [37] G. Boulon, *Opt. Mater.* 22 (2) (2003) 85–87.
- [38] A. Brenier, *J. Luminesc.* 92 (3) (2001) 199–204.